OPEN ACCESS
Jurnal Ilmiah Ilmu Terapan Universitas Jambi
Vol. 10 No. 2. April 2026, pp. 804-822 DOI. 10.22437/jiituj.v10i2.54453
Research Article

MINERALOGICAL ANALYSIS OF ROCK WEATHERING AND ITS INFLUENCE ON SLOPE FAILURE ALONG THE JAYAPURA CITY RING ROAD

Enos Karapa[1*], Joni[2], Endang Hartiningsih[3], Marcelino Novryanto Yonas[4], Rahmat Indrajati[3], Djuarensi Patabang[4], Nur Ayu Anas[3]
[1]Department of Mining Engineering, Cenderawasih University, Jayapura 99351, Indonesia
[2]Department of Renewable Energy Engineering, Graduate School of Cenderawasih University, Jayapura 99351, Indonesia
[3]Department of Geological Engineering, Cenderawasih University, Jayapura 99351, Indonesia
[4]Department of Mineral Engineering, Graduate School of Cenderawasih University, Jayapura 99351, Indonesia
Corresponding author email: enos_karapa@ftuncen.ac.id

Article Info
Recieved: Feb 2, 2026
Revised: Mar 15, 2026
Accepted: Apr 15, 2026
OnlineVersion: Apr 29, 2026

Abstract
Slope failure along the Jayapura City Ring Road persisted despite shotcrete reinforcement, indicating that instability is not controlled solely by slope geometry or surface confinement. Field evidence points to weakening within foliated metamorphic rocks affected by tropical weathering, where mineral alteration progressively modifies the internal structure. This study examines how mineralogical transformations govern subsurface degradation and contribute to failure beneath reinforced slopes. A case study approach was applied using two representative samples (ST-01 and ST-02) obtained directly from the failure zone. Petrographic analysis of ~30 µm thin sections was conducted to evaluate mineral textures, fabric orientation, and alteration pathways. X-ray diffraction (XRD) was used to identify and semi-quantify the mineral phases, including albite, quartz, chlorite, muscovite, sericite, and magnetite. Subsurface conditions were assessed using ADMT resistivity profiling across a frequency range of 0.0001–10,000 Hz, reaching depths of approximately 300 m. The results indicate a mineralogical transition from a wollastonite–actinolite–chlorite assemblage in ST-01 to a chlorite–muscovite–sericite-dominated system in ST-02. The XRD data show a decrease in albite from ~19.74% to ~11.61%, while an unresolved fraction exceeding ~20% suggests the presence of poorly crystalline phases. Petrographic observations revealed that chlorite and sericite were concentrated along foliation and microfractures. The resistivity data identified a low-resistivity zone (10–20 Ωm) at depths of ~10–60 m, corresponding to altered and fluid-influenced domains. These findings indicate that weathering reduces cohesion along structurally controlled planes while preserving partial framework integrity, shifting the locus of failure to the subsurface beneath the shotcrete layer.

Keywords: Chlorite–Muscovite, Petrography, Phyllosilicate, Resistivity, Rock Weathering

INTRODUCTION

Slope instability in tropical mountainous corridors cannot be adequately interpreted using geometric parameters alone (Gofar et al., 2025). In humid environments, the mechanical conditions of rock masses evolves progressively under the influence of water infiltration, mineral dissolution, and fabric degradation, often well before visible deformation occurs. This issue becomes more complex in slopes reinforced with shotcrete, where the external surface may remain intact while internal weakening continues (Chen et al., 2020; Tang et al., 2020; Yan et al., 2020). Field observations along the Jayapura City Ring Road indicate that several reinforced slopes experienced failure despite surface protection, suggesting that the controlling mechanism operates beneath the shotcrete layer rather than at the exposed face.

From a mechanistic standpoint, slope degradation in such environments is better understood as a coupled hydro–chemo–mechanical process rather than a purely mechanical one. In foliated metamorphic rocks, the internal fabric governs the fluid pathways, stress redistribution, and damage localization. Experimental studies have shown that the compressive strength varies systematically with foliation orientation ($\theta = 0°–90°$), producing anisotropic responses that directly influence the failure behavior (Waqas et al., 2024; Yan et al., 2020). This anisotropy is dynamic in nature that tends to increase when chemical weathering modifies the mineral bonds and microstructures. For instance, exposure of dioritic rocks to acidic conditions for 49 days has been shown to increase microcrack density and generate flocculent textures, while reductions in pH from 7 to 5 and 3 resulted in peak strength decreases of 16.6% and 11.92%, accompanied by elastic modulus reductions of 25.36% and 23.13% (Erharter, 2024; B. Liu et al., 2021; Mader et al., 2022; Y. Wang et al., 2022; Yin et al., 2023). These values indicate that chemical alterations introduce measurable and cumulative degradation.

A critical transition occurs when weathering promotes the formation of phyllosilicate-rich assemblages, such as chlorite, muscovite, and sericite. These minerals tend to concentrate along foliation planes and fractures, where they reduce cohesion more significantly than they do frictional resistance. Experimental and geochemical studies suggest that clay-related alterations preferentially weaken intergranular bonding, effectively transforming the rock mass into a system dominated by planar slip surfaces rather than interlocking (Bonnet et al., 2024; Cui et al., 2025; J. Liu et al., 2022; H. Zhang et al., 2025). In practical terms, rocks may retain their macroscopic structure while losing internal mechanical continuity. This condition is particularly relevant in foliated metamorphic terrains, where structural anisotropy predisposes the rock mass to directional failure (Zheng et al., 2026).

Although previous studies have quantified strength reduction, anisotropy, and mineral transformation, these aspects are often considered separately. Mineralogical alteration is frequently described as a secondary characteristic rather than an active control of slope performance. Consequently, the interaction between mineral-scale processes and engineered reinforcement systems remains insufficiently resolved. In shotcrete-reinforced slopes, this gap is critical because the reinforcement is typically designed based on surface conditions and geometric stability, whereas subsurface mineralogical degradation is rarely incorporated into assessment frameworks. This creates a potential mismatch between the apparent stability at the surface and the actual mechanical integrity at depth.

The Jayapura City Ring Road provides a representative case in which this mismatch is evident. The slope is developed in foliated metamorphic rocks subjected to intense tropical weathering, conditions that favor mineralogical transformation along structurally controlled pathways. Petrographic observations indicate that alteration products are concentrated along foliation and microfractures, whereas X-ray diffraction (XRD) results reveal a transition toward phyllosilicate-dominated assemblages (Sirbu-Radasanu et al., 2022). In parallel, the resistivity data identified a conductive zone at depths of approximately 10–60 m, characterized by low resistivity values of 10–20 Ωm, which are commonly associated with clay enrichment, fluid circulation, and reduced rock competence. The coexistence of these features suggests that weakening is not confined to the surface but is embedded within the rock mass (Starr & Pattison, 2019; H. Wang et al., 2019).

Despite these observations, a key question remains insufficiently addressed: to what extent does mineralogical alteration control slope failure beneath shotcrete reinforcement, and how can this process be detected and interpreted before failure occurs? Existing approaches tend to rely on either geotechnical parameters or geophysical indicators. However, the integration of petrography, X-ray diffraction (XRD), and resistivity data to trace the pathway from mineral transformation to mechanical failure has been less explored.

This study aims to treat mineralogical processes as mechanistically relevant variables and focuses on two representative samples (ST-01 and ST-02) obtained from a failed slope segment, examined using an integrated analytical framework combining petrography, X-ray diffraction (XRD), and resistivity interpretation. The analysis includes: (1) identifying how weathering modifies mineral assemblages and rock fabric in foliated metamorphic rocks; (2) evaluating how these changes influence mechanical weakening beneath shotcrete reinforcement; and (3) determining whether low-resistivity anomalies correspond to zones of subsurface degradation. The working hypothesis assumes that progressive weathering promotes phyllosilicate enrichment along foliation-controlled discontinuities, which in turn reduces cohesion and shifts the locus of failure from the surface to the subsurface; slope instability therefore appears less dependent on external loading or geometry and more closely associated with an internally evolving weakening process governed by mineralogical transformation.

RESEARCH METHOD

Research Design and Sampling Technique

This study adopted a case-study design with an integrated field–laboratory approach to examine the relationship between rock weathering, mineralogical alteration, and slope failure along the Jayapura City Ring Road in eastern Indonesia. The sampling strategy was purposive rather than randomized. Two representative rock blocks, designated ST-01 and ST-02 (Figure 1), were selected directly from the failure zone of the shotcrete-reinforced slope based on three criteria: the visible weathering intensity, lithological variation, and proximity to the damaged slope surface. This sampling logic was appropriate because the purpose of the study was to characterize the failure mechanism of a specific slope segment rather than to estimate population-level parameters across multiple slopes.

Figure 1. Rock samples

The study site is located at 2°35'24.87" S and 140°41'31.60" E (Figure 2) at an elevation of approximately 29 m above sea level. The field inspection documented the slope geometry, foliation orientation, fracture development, surface deterioration, and distribution of the shotcrete damage. These observations were used to define the failure zone and guide the sample extraction from the most affected material.

Figure 2. Research location

Analytical Strategy

The analysis was built around geological triangulation rather than latent-variable modeling. Therefore, statistical packages designed for survey-based structural equation modeling, were not used (Price, 2016). These tools are suitable when the data consist of questionnaire items, latent constructs, or covariance structures. In this study, data were obtained from a physical slope system and generated through resistivity profiling, petrographic examination, and X-ray diffraction (XRD). Therefore, the appropriate interpretation framework was mineralogical and geophysical, rather than psychometric.

The analytical sequence was as follows: First, the resistivity data were interpreted to identify conductive intervals associated with the fracture concentration, water influence, or clay enrichment. Second, petrographic analysis was used to determine the rock texture, fabric, alteration minerals, and replacement relationships. Third, XRD was used to confirm the crystalline mineral phases and estimate their relative abundances. Finally, the three datasets were integrated to evaluate whether the slope failure was primarily governed by weathering-induced mineralogical weakening beneath the shotcrete layer.

Variable Definition and Operational Measurement

Because this study is framed as a geological case, the analysis of parameters is approached as concrete expressions of slope behavior, features that can be traced in outcrops, thin sections, or resistivity responses, rather than as abstract variables detached from their physical context. Each parameter, in this sense, corresponds to a condition that can be directly observed or reasonably inferred, whether through field inspection or laboratory examination. To avoid treating these elements as isolated descriptions, they were arranged into a structured set of descriptors that link slope conditions with observable indicators and the methods used to capture them. The relationships among slope failure characteristics, weathering intensity, rock fabric, mineralogical composition, and subsurface weak zones are summarized in Table 1, which outlines how each parameter is defined and operationalized within the analytical workflow.

Table 1. Variable and operational descripton

Variable	Operational definition	Indicator	Measurement / source
Slope failure condition	Physical instability of the shotcrete-reinforced slope	Cracking, detachment, localized collapse, and exposed weakened zones	Direct field observation at the failure location
Weathering intensity	Degree of mineralogical and textural alteration in the rock mass	Secondary mineral development, fracture infill, replacement textures, and discoloration	Petrographic thin-section examination
Rock fabric	Internal structural arrangement of the metamorphic rock	Foliation, schistosity, lepidoblastic texture, and porphyroclastic texture	Polarizing microscope observation
Mineralogical composition	Crystalline phases present in each sample	Primary minerals and alteration products such as chlorite, muscovite, sericite, quartz, albite, and magnetite	Petrography and XRD phase identification
Subsurface weak zone	Conductive interval associated with altered or fractured material	Low resistivity values	ADMT resistivity profiling in Ωm
Alteration intensity beneath shotcrete	Extent of weathering below the reinforcement layer	Spatial overlap between conductive anomaly and altered mineral assemblage	Integrated interpretation of resistivity, petrography, and XRD

As outlined in Table 1, each variable is intentionally tied to a specific observational or analytical approach, allowing the interpretation to remain grounded in measurable geological evidence rather than inferred constructs. For instance, slope failure is identified through direct field indicators such as cracking and detachment, whereas weathering intensity is interpreted from petrographic features like mineral replacement and fracture infill.

Resistivity Measurement

Resistivity measurements were conducted using an ADMT 3000-HT (Figure 3) system with an effective investigation depth of up to ~300 m, depending on the signal penetration and the local subsurface conductivity. This method relies on naturally occurring electromagnetic (EM) fields and records orthogonal electric (E) and magnetic (H) components in the frequency domain at the Earth's surface. The subsurface resistivity is inferred from frequency-dependent variations in these field responses. The EM spectrum utilized spans approximately 0.0001–10,000 Hz, where high-frequency components (>1 Hz) are primarily associated with lightning activity, intermediate frequencies (<1 Hz) with ionospheric resonance, and low-frequency signals (≪1 Hz) with solar-induced variations (Grayver, 2024). As EM fields propagate into the ground, conductive heterogeneities generate secondary (eddy) currents that are detected and used to reconstruct resistivity profiles. The interpretation assumes plane wave propagation, with mutually perpendicular E and H fields and is governed by Maxwell's equations (Barajas-Olalde et al., 2023; Castillo-Reyes et al., 2025).

Figure 3. ADMT 3000-HT type reisistivity instrument

Petrographic Analysis

Two representative samples, ST-01 and ST-02, were prepared as thin sections for petrographic analysis using a Nikon Eclipse LV600D polarizing microscope (Figure 4). Thin-section preparation followed standard laboratory procedures, including cutting, mounting, grinding, and polishing of the samples. Rock fragments were bonded to glass slides using Petropoxy 154 and ground to a thickness of approximately 30 μm using a Maruto ML-110NT system. Carborundum and fine alumina were used during the abrasive stages, followed by diamond paste polishing to produce optical transparency under transmitted light.

Figure 4. Process of petrographic analysis

Petrographic analysis was used to identify primary and secondary mineral assemblages, mineral habits, foliation, alteration products and textural relationships. The main purpose of this analysis was to

determine how weathering modified the rock fabric and whether the alteration products were concentrated along structurally weak planes, such as foliation and micro-fractures (De Oliveira Frascá, 2018; Mitchell & Sass, 2024).

X-ray Diffraction (XRD) Analysis

XRD analysis was conducted using a Shimadzu XRD-7000L diffractometer (Figure 5) at the Integrated Laboratory of the Faculty of Engineering, Hasanuddin University. The rock fragments were crushed in an agate mortar, sieved through a #200 mesh (<0.075 mm), oven-dried, and packed into sample holders to obtain a flat and homogeneous surface. Diffraction data were collected over a 2θ range of approximately 5°–70° using Cu-Kα radiation (Nzeukou et al., 2024). The observed peaks were matched with standard reference patterns from the ICDD database to identify the mineral phases. The relative phase abundance was estimated semi-quantitatively from the peak intensity and area, with the interpretation made cautiously because the preferred orientation and grain size effects can affect the diffraction behavior (Döbelin, 2020; Park et al., 2026; Xiao et al., 2023).

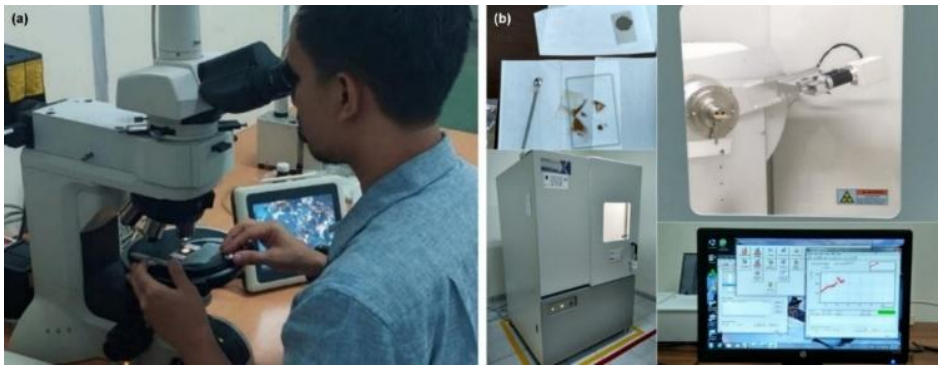

Figure 5. (a) Nikon Eclipse Type LV 600D polarizing microscope instrument, and (b) Shimadzu XRD-7000L instrument.

XRD was necessary in this study because petrography alone does not fully capture fine-grained or poorly crystalline phases. This method added a quantitative layer to the interpretation by confirming the presence of albite, quartz, chlorite, muscovite, sericite, and magnetite, as well as a notable fraction of the unresolved phases.

Instrument Validation and Reliability

Instrument validity was established using cross-methods confirmation. The resistivity anomaly was not interpreted in isolation; it was checked against the petrographic fabric and X-ray diffraction (XRD) mineralogical data. This reduced the risk of assigning failure to a single geophysical response without mineralogical support. In practical terms, the validity of the interpretation rested on the agreement among three independent lines of evidence: subsurface conductivity, mineral replacement, and the crystalline phase composition.

Reliability was addressed through standardized sample preparation and consistent identification criteria. Thin sections were prepared using the same laboratory procedure for both samples, and XRD phase identification followed a fixed reference-matching protocol against the ICDD database (Kiselnikov et al., 2026). Because the study did not use questionnaire items or multi-item scales, internal consistency measures such as Cronbach's alpha were not applicable. In this design, reliability depends on repeatable preparation, controlled observation, and stable interpretation rules rather than item correlation statistics.

Data Integration

The interpretation combined field observations, resistivity patterns, petrographic textures and XRD mineralogical data. Resistivity data were used to map subsurface contrasts in material competence and water influence; petrography was used to document deformation fabrics, alteration pathways, and mineral replacement; and XRD was used to quantitatively verify mineral assemblages (Tao et al., 2024; Yamasaki & Chigira, 2007). The integration of these datasets provided the basis for evaluating whether slope failure was primarily controlled by weathering-related mineralogical weakening beneath the shotcrete layer.

RESULTS AND DISCUSSION

Mineralogical Processes as Mechanistic Variables

This study treats mineralogical processes as mechanistically relevant variables rather than descriptive background conditions. Two representative samples, ST-01 and ST-02, were collected from the failed slope segment and examined using an integrated framework combining petrography, XRD, and resistivity interpretation. The analysis was directed toward three linked questions: how weathering modifies mineral assemblages and rock fabric in foliated metamorphic rocks, how these changes contribute to mechanical weakening beneath shotcrete reinforcement, and whether low-resistivity anomalies correspond to zones of subsurface degradation (McAleer et al., 2017; X.-Z. Zhang et al., 2017). The working hypothesis assumes that progressive weathering promotes phyllosilicate enrichment along foliation-controlled discontinuities, reducing cohesion and shifting failure from the surface to the subsurface (Uzarowicz et al., 2012). In this sense, instability is interpreted less as a response to external loading or slope geometry alone and more as the outcome of an internally evolving weakening process governed by mineralogical transformation. This framing is consistent with the broader view that tropical slope failure in weathered rock masses is rarely a purely geometric problem because water infiltration, fabric degradation, and mineral alteration can reorganize mechanical behavior long before collapse becomes visible at the surface.

Petrographic Degradation of Structures

The thin-section photomicrograph of ST-01 (Figure 6) shows a foliated metamorphic rock in which deformation and alteration are already coupled at the mineral scale. Wollastonite (W_o) and actinolite (A_{ct}) remain visible as structurally significant phases, but their grain boundaries are not entirely sharp, and several contacts appear diffuse, suggesting re-equilibration during progressive deformation and weathering. Quartz (Q_z) occurs as anhedral grains with irregular margins, while chlorite (C_{hl}) develops preferentially along foliation planes, grain boundaries, and microfractures (Mu et al., 2023; Nzeukou et al., 2024; J. Wang et al., 2025; Zalooli et al., 2024). This distribution matters because the alteration is not dispersed randomly through the rock; instead, it is concentrated along the very planes that already function as mechanical discontinuities. Albite (A_b) preserves twin structures but also exhibits internal fractures, some of which are filled by fine material, indicating that fluid circulation accompanied fracturing (Adjo et al., 2021; Arango-Escobar et al., 2021). At later stages, sericite (S_{er}) becomes more prominent, coating feldspar and quartz surfaces as very fine aggregates, and opaque minerals interpreted as magnetite (O_{pq}) are disseminated in altered domains. These conditions indicate a weathering pathway in which fluid access follows foliation and microfractures, progressively transforming a more coherent metamorphic fabric into a weaker mass of anisotropic rocks (Astakhova et al., 2021; Maruyama et al., 1983; Rösche et al., 2022; Sirbu-Radasanu et al., 2022).

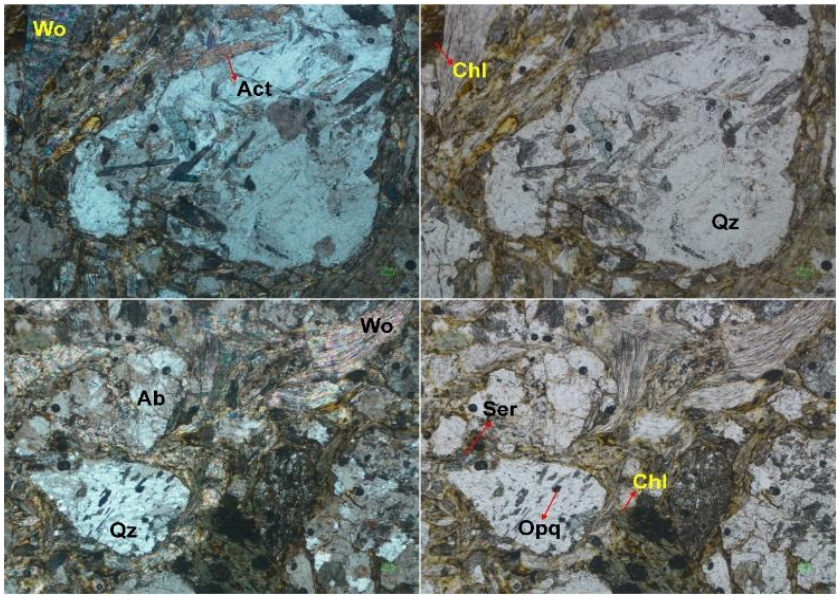

Figure 6. Photomicrograph of a thin section of sample ST-01.

Table 2 supports this interpretation by showing that ST-01 still retains a substantial proportion of framework minerals: wollastonite (25%), actinolite (18%), albite (20%), chlorite (17%), sericite (10%), quartz (5%), and opaque minerals (<5%). The presence of wollastonite and actinolite in appreciable amounts indicates that the rock has not yet undergone a complete mineralogical collapse. However, the coexistence of chlorite and sericite along foliation and fracture zones suggests that alteration has already started to reorganize the internal structure. In mechanical terms, the rock is still partly supported by interlocking crystalline phases, but its effective continuity is increasingly interrupted by phyllosilicate-filled surfaces. This distinction is important because a rock mass can preserve an apparently intact outcrop expression while already losing cohesion along its weakest planes. This pattern is consistent with foliated metamorphic rocks exposed to tropical weathering, where mineral transformation advances along pre-existing anisotropy rather than uniformly across the fabric.

Table 2. Composition of mineral in sample ST-01

Composition of Mineral	Amount (100%)	Description of Optical Mineralogy
Wollastonite (Wo), $CaSiO_3$	25%	Transparent absorption color (colorless) with purplish green interference color, moderate relief, weak intensity, columnar-fibrous shape, first order birefringence, no pleochroism (-), darkness angle 24-37º, oblique darkness type, mineral size 0.04-1.2 mm.
Actinolite (Act) $Ca_2(Mg,Fe^{2+})_5Si_8O_{22}(OH)_2$	18%	Brownish absorption color with pale green interference color, medium relief, weak intensity, flat/needle-shaped, bidirectional cleavage, weak-moderate pleochroism, darkening angle 10-15º, oblique darkening type, mineral size 0.08-1.5 mm
Quartz (Qz), SiO_2	5%	Transparent (colorless), no pleochroism (-), low intensity, sub-anhedral shape, low relief, no cleavage, conchoidal fracture, mineral size <1 mm, no twinning, darkness angle 2-5°.
Albite (Ab), $NaAlSi_3O_8$	20%	Transparent (colorless) with brownish interference patterns, measuring 0.4-2 mm, sub-anhedral. Some features show calcbad-albite twinning, a 15-21º darkening angle, and an oblique darkening type. Large individual crystals have fractures that follow cleavage planes and some are irregular.
Chlorite (Chl), $(Mg, Al,Fe)_3(Si,Al)_4O_{10}(OH)_2(Mg,Al,Fe)_3(OH)_6$	17%	Green-brownish black in color, microgranular-fibrous in shape, the result of mafic mineral alteration (cleavage, edge, and fracture mineral parts).
Opaque Minerals (Opq) / Magnetite (Mag) Fe_3O_4	<5%	Black in color, isotropic (not translucent), mineral size <1 mm, partly cubic or granular, indicated as magnetite mineral.
Sericite (Ser), $KAl_2(AlSi_3O_{10})(OH)_2$	10%	Transparent (colorless), in the form of fine fibers on the surface of silica minerals (<0.02 mm), and some have been oxidized.

The photomicrograph of ST-02 (Figure 7) shows a more advanced stage of reorganization. In this sample, the fabric is denser, the foliation is more continuous, and the dominant minerals are muscovite (M_s) and chlorite (C_{hl}), both aligned parallel to the deformation planes. Quartz remains present, but it is less influential in shaping the fabric than the phyllosilicate phases (Yan et al., 2020; Zhou et al., 2020). Albite (A_b) still displays twinning, yet the grains are more disturbed, and several are fractured or partially fragmented. Sericite (S_{er}) occurs as a later-stage alteration product coating feldspar and quartz surfaces, while magnetite (Mag) appears as fine opaque grains associated with altered zones (Habimana & Sauvé, 2025; Zalooli et al., 2024). This assemblage is not merely a compositional shift from ST-01 to ST-02; it signals a deeper change in how the rock resists stress. In ST-01, the rock still retains a mixed framework of relatively competent silicates and alteration products. In ST-02, the balance has moved toward aligned sheet silicates, which favor slip along foliation and reduce intergranular locking. As a result, the

mechanical response becomes more anisotropic and more sensitive to moisture, stress orientation, and continued alteration.

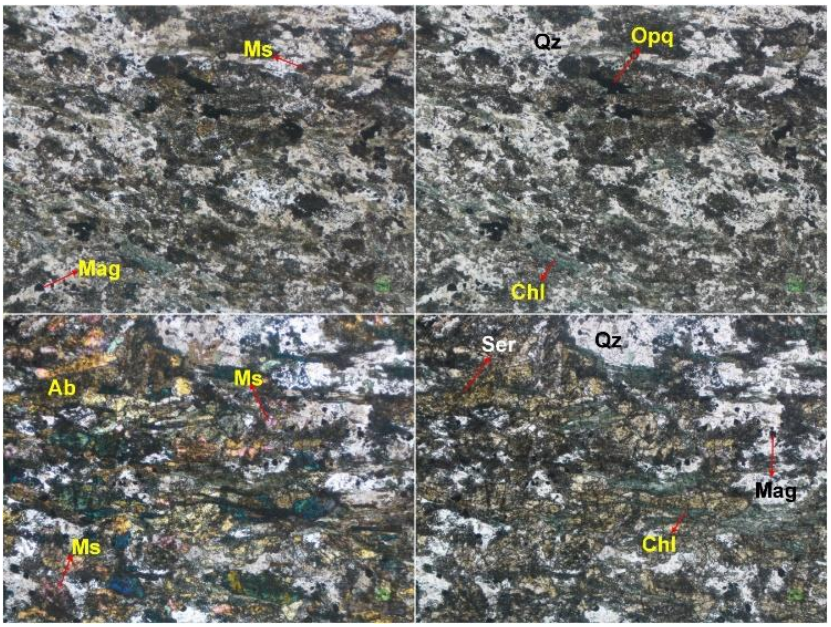

Figure 7. Photomicrograph of a thin section of sample ST-02.

Table 3 clarifies that ST-02 is dominated by muscovite (28%), quartz (21%), sericite (19%), albite (15%), chlorite (15%), and opaque minerals (2%). Compared with ST-01 the increase in muscovite and sericite is especially significant because both minerals are platy and mechanically weak along their basal surfaces. Their abundance implies that alteration has progressed from partial replacement into a fabric where foliation itself is increasingly defined by low-strength minerals. That transformation likely reduces cohesion more than friction angle. In other words, the rock may still resist sliding under dry, confined conditions, but its internal bonds are now weaker and less able to maintain integrity once fluid pressure rises or loading is redistributed foliation plane and edges of individual minerals (Adjo et al., 2021).. The microstructural evidence therefore supports classification of ST-02 as a chlorite–muscovite schist with stronger weathering overprint than ST-01, and it suggests that the failure process is already embedded in the rock fabric before any visible surface collapse occurs.

Table 3. Composition of mineral in sample ST-02

Composition of Mineral	Amount (100%)	Description of Optical Mineralogy
Albite (Ab), $NaAlSi_3O_8$	15%	Transparent (colorless) with brownish interference colors, measuring 0.2-1.85 mm, sub-anhedral in shape. Some features show calsbad-albite twinning, a 12-20º darkening angle, and an oblique darkening type. In individual large crystals, fractures occur that follow cleavage planes and some are irregular.
Quartz (Qz), SiO_2	21%	Transparent (colorless), no pleochroism (-), low intensity, sub-anhedral shape, low relief, no cleavage, conchoidal fracture, mineral size 0.05-1 mm, no twinning, darkness angle 1-3°.
Muscovite (Ms), $KAl_2(AlSi_3O_{10})(OH)_2$	28%	Transparent absorption color (colorless) with purplish green interference color, medium relief, weak intensity, flat shape, two-way cleavage, dichroic pleochroism, darkness angle 21-34º, oblique darkness type, mineral size 0.06-1.5 mm.
Chlorite (Chl), $(Mg, Al,Fe)_3 (Si,Al)_4O_{10} (OH)_2 (Mg,Al,Fe)_3 (OH)_6$	15%	Green-brownish black in color, microgranular-fibrous (fine fibers), the result of mafic mineral alteration (cleavage, edge, and fracture mineral parts).

Composition of Mineral	Amount (100%)	Description of Optical Mineralogy
Opaque Minerals (Opq) / Magnetite (Mag) Fe_3O_4	2%	Black in color, isotropic (not translucent), mineral size <1 mm, partly cubic or granular, indicated as magnetite mineral.
Sericite (Ser), $KAl_2(AlSi_3O_{10})(OH)_2$	19%	Transparent (colorless), in the form of fine fibers on the surface of silica and muscovite minerals (<0.02 mm), and some have been oxidized.

Mineral Composition Based on X-ray diffraction (XRD) Analysis

The XRD results shown in Figures 8 and 9 provide the quantitative counterpart to the petrographic observations. In ST-01, the principal phases were approximately albite 19.74%, chlorite 14.24%, quartz 3.16%, and magnetite 3.16%, accompanied by an unidentified fraction of 20.56%. In ST-02, the phase distribution changes to albite 11.61%, quartz 5.87%, muscovite 3.52%, chlorite 2.68%, magnetite 1.46%, and an unidentified fraction of 20.28%. The shift is not dramatic in the sense of complete mineral replacement, but it is mechanically significant. Albite decreased from 19.74% to 11.61%, chlorite decreased from 14.24% to 2.68%, and muscovite appeared in the second sample. These numbers indicate a more advanced reorganization of the mineral system in ST-02, where the original framework minerals have been increasingly overprinted by secondary phyllosilicates (J. Liu et al., 2022).

The unresolved fraction above 20% in both samples requires particular attention. In a tropical weathering profile, such a proportion is unlikely to be treated as minor laboratory residual. This more plausibly represents poorly crystalline products, mixed-layer clays, or amorphous alteration phases that standard diffraction cannot resolve cleanly (Aydan et al., 2023). That interpretation is consistent with thin-section evidence showing fine-grained alteration along foliation planes and fractures. The key point is that part of the rock mass may have moved away from a stable crystalline configuration while still retaining enough silicate structure to appear coherent in hand samples. In other words, XRD does not show a total breakdown; it shows partial preservation of a crystalline framework inside a broader alteration field. This condition often precedes strength degradation without immediate macroscopic collapse. Similar behavior has been reported where clay minerals are chemically altered without producing sharply distinct new phases, yet still weaken cohesion and modify water sensitivity at the rock scale (Aydan et al., 2023; Bonnet et al., 2024; Erharter, 2024).

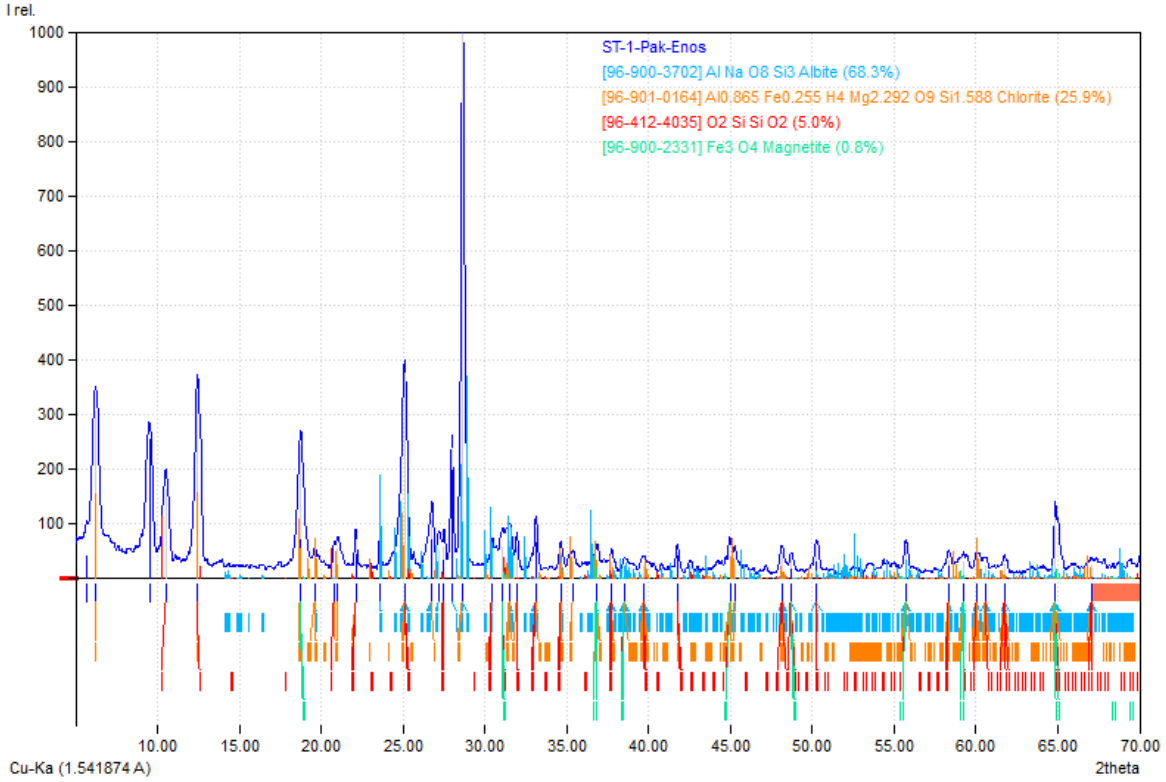

Figure 8. XRD analysis results of sample ST-01

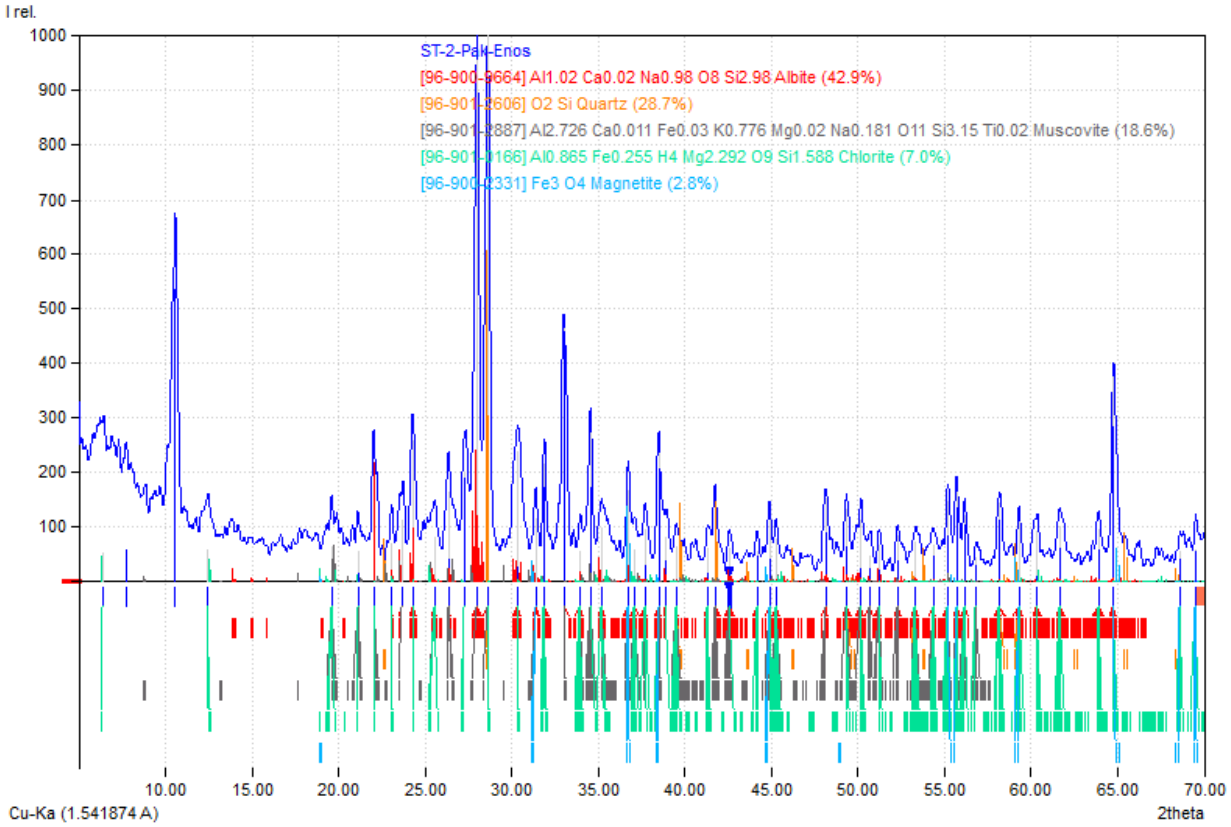

Figure 9. XRD analysis results of sample ST-02

A mechanical reading of the XRD data also clarifies the role of phyllosilicates. Even when their percentage is not dominant, chlorite and muscovite can control shear behavior because sheet silicates promote slip along preferred crystallographic planes. Their influence is amplified in foliated rocks, where the mineral plates align with pre-existing anisotropy. That is why the 14.24% chlorite in ST-01 is more important than the number alone suggests, and why the combined muscovite–chlorite–sericite presence in ST-02 is critical even though muscovite appears at only 3.52% in the XRD pattern. The spatial arrangement of those phases along foliation planes is likely to reduce frictional interlocking and effective cohesion more than their bulk abundance would imply. Experimental studies cited in the manuscript show that discontinuities enriched in platy minerals commonly develop lower static friction coefficients and stronger orientation dependence in strength behavior (Aydan et al., 2023; Erharter, 2024). The Jayapura samples follow that logic closely.

The mineralogical trend from ST-01 to ST-02 also supports the progressive reduction in framework stability. Albite remained present in both samples, but its decline from 19.74% to 11.61% points to the continued weathering of a more resistant feldspathic phase. Quartz increased slightly from 3.16% to 5.87%, this increase did not offset the broader shift toward a phyllosilicate-rich fabric. Quartz is mechanically competent, but does not compensate for the weakening effect of aligned chlorite, muscovite, and sericite along foliation and fracture planes. The relevant issue is not whether silicate minerals remain present; they do remain. This is because the intergranular network becomes less effective at carrying stress. In this sense, the XRD data suggest a rock mass that is still mineralogically recognizable but mechanically less integrated. This distinction is central for evaluating reinforcement performance on weathered metamorphic slopes.

The combined petrographic and XRD evidence indicates that weathering in the Jayapura slope primarily reduced cohesion rather than immediately collapsing the internal friction angle. This distinction is important because a slope may still appear resistant under dry or low-disturbance conditions while already carrying much lower residual bonding strength along foliation-parallel surfaces. In ST-01, the fabric retained a mixed mineral architecture, with wollastonite and actinolite contributing to the structural support. In ST-02, however, the alignment of muscovite, chlorite, and sericite created a more continuous anisotropic network. Once those phyllosilicates are connected along foliation and fracture zones, deformation localizes more readily, and the rock mass begins to respond as a sheeted material rather than

a granular interlocked aggregate. This shift is mechanically more important than a simple change in the modal mineral percentages.

The distinction between cohesion and frictional losses is also supported by the alteration style. The manuscript notes that chemical weathering under acidic or fluid-active conditions tends to weaken mineral bonds, increase microcrack density, and lower peak strength more rapidly than it changes the friction angle. The cited studies reported peak strength reductions of 16.6% and elastic modulus losses of 25.36% under increasingly acidic conditions, indicating that mineral corrosion can substantially degrade structural performance even before total disintegration occurs (Chen et al., 2020; J. Liu et al., 2022; Y. Wang et al., 2022). The Jayapura samples fit this pattern: the rock remains coherent enough to preserve foliation, yet its intergranular bonding has been undermined by alteration products concentrated along weak surfaces. The result is a mechanically weaker mass whose failure tendency increases without a dramatic change in its outward appearance.

This weathering trajectory is important because it shows how a foliated metamorphic rock can transition from a relatively competent state to a condition in which deformation is strongly plane-controlled. This process is gradual rather than sudden. However, gradual does not imply insignificant. Once chlorite, muscovite, and sericite become continuous along the foliation, the rock no longer resists load in a uniform manner. Instead, it develops a directional weakness that depends on the fabric orientation, moisture state, and stress redistribution. The literature cited in the manuscript repeatedly shows that joint orientation, fabric anisotropy, and transversely isotropic behavior can dominate the rock mass response in both natural slopes and engineered excavations (B. Liu et al., 2021; Mader et al., 2022; Yin et al., 2023). Therefore, the Jayapura slope therefore belongs to a class of failures in which the internal structure, rather than the surface geometry, dictates instability.

Resistivity Anomalies and Identification of Subsurface Degradation

The resistivity data in Figure 10 add the subsurface dimension that the petrographic and XRD results cannot provide alone. The profile shows three main resistivity ranges: 10–20 Ωm, 20–40 Ωm, and 40–52 Ωm. The most consequential feature is the low-resistivity interval at a depth of approximately 10–60 m depth, which persists across the measured sections. In foliated metamorphic terrains, such values are commonly associated with conductive fluids, clay enrichment, fracture networks, and weathered material. Here, the spatial coincidence between low resistivity and the mineralogical signatures of alteration supports a reading in which the 10–60 m interval marks a chemically and mechanically weakened domain. Therefore, the profile is not just a water-saturation map. This is a signal of subsurface reorganization in which conductivity and weakening are coupled.

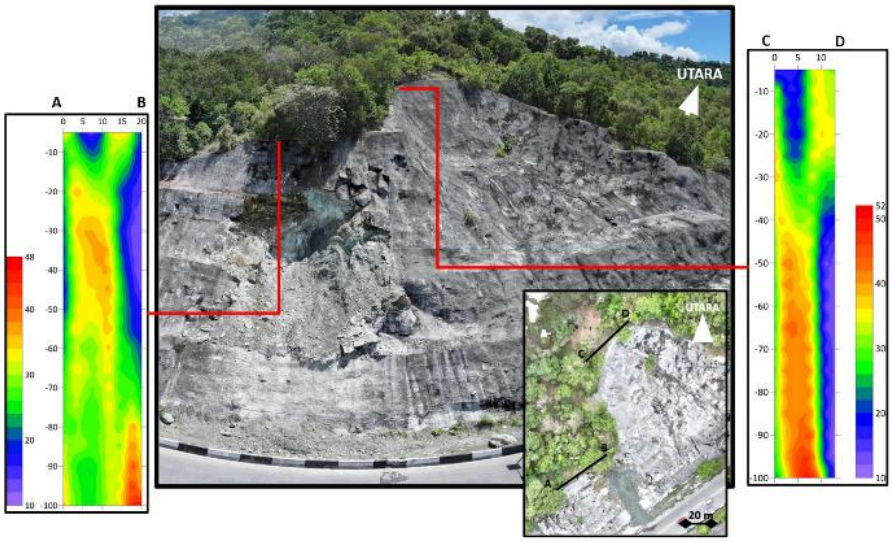

Figure 10. Vertical resistivity values

This interpretation becomes stronger when the resistivity pattern is compared with the XRD and petrographic evidence. ST-01 and ST-02 both contain substantial alteration products, but ST-02 is more strongly overprinted by muscovite, chlorite, and sericite, which implies that the low-resistivity zone likely corresponds to a mineralogically transformed horizon rather than a simple wet zone (Liang et al., 2023;

Phyu et al., 2021; H. Zhang et al., 2025). In weathered rocks, conductive intervals in the 10–20 Ωm range often mark clay-rich or fracture-saturated material, whereas values of 20–40 Ωm represent transitional zones where some framework integrity remains, and 40–52 Ωm usually indicate comparatively intact rock (Sun et al., 2020; Waqas et al., 2024). The Jayapura slope fits this stratification. The point is not that resistivity alone proves the mineralogy; it does not. The resistivity anomaly is spatially consistent with the observed alteration style and therefore provides a credible proxy for internal weakness.

The mechanical implications are direct and straightforward. A low-resistivity interval at 10–60 m depth suggests a zone where permeability, fluid circulation, and alteration have likely interacted to reduce the stiffness and continuity. This interval is particularly important because it lies below the effective influence of surface shotcrete (Yan et al., 2020; Yang et al., 2026; Zhou et al., 2020). The conductive zone should not be understood not merely as a water-bearing layer, but as a structure. The reinforcement can confine the exposed face, but it cannot restore the deeper rock fabric once the internal cohesion is reduced by weathering and clay-like phase development. In practical terms, the slope can remain visually protected while its substrate becomes progressively less capable of carrying the load. This is a structural decoupling problem: the support system acts at the surface, whereas the failure mechanism develops below it. Similar situations have been reported on other altered slope systems, where the rock mass quality is time-dependent and changes as mineral transformation advances (Baldermann et al., 2021; Phyu et al., 2021; Siddique, 2024).

Mechanism of failure beneath shotcrete reinforcement

The failure observed along the Jayapura City Ring Road is more convincingly explained as a subsurface weathering-driven failure rather than a simple deficiency of surface reinforcement. Petrographic data show that alteration is concentrated along foliation planes and microfractures. The XRD data show that the mineral system is shifting toward phyllosilicate-rich assemblages, especially in ST-02. The resistivity profile revealed a conductive interval at 10–60 m depth which is consistent with fluid influence and mineralogical weakening. These three lines of evidence converge on the same mechanism: the rock mass is losing internal continuity from within, while the shotcrete layer remains relatively intact at the surface. That condition produces a dangerous mismatch between visible stability and the actual mechanical condition (Kiselnikov et al., 2026; Regmi et al., 2013).

Chlorite, muscovite, and sericite are not simply mineral labels in analytical tables. Their sheet-like structure promotes slip, lowers interlocking efficiency, and reduces shear resistance along the aligned planes. In foliated rocks, this is amplified because these minerals naturally occupy the same fabric surfaces that already serve as mechanical discontinuities. The consequence is a slope whose internal strength becomes direction dependent. Under such circumstances, even moderate rainfall, fluid ingress, or stress redistribution may be sufficient to activate failure along a pre-weakened zone. The literature cited in the manuscript emphasizes this behavior: phyllosilicate enrichment lowers frictional resistance, weathering reduces cohesion, and anisotropic fabric controls where deformation localizes (Aydan et al., 2023; Liang et al., 2023; B. Liu et al., 2021; Mader et al., 2022). The Jayapura slope displayed the same pattern, but in a field setting where the surface shotcrete obscured the deeper degradation process.

ST-01 still contained 25% wollastonite, 18% actinolite, and 20% albite, indicating that the rock retained a substantial framework of relatively competent mineral phases. In contrast, ST-02 is composed of 28% muscovite, 19% sericite, 15% chlorite, and only 15% albite, reflecting a more altered and mechanically weaker fabric. The difference is not merely compositional, but also organizational. In ST-02, phyllosilicates are more continuously aligned along foliations, allowing the rock mass to deform through slip along low-strength planes rather than resisting deformation through interlocking grains. This condition indicates a structurally controlled instability, such that slope performance should not be assessed solely based on the external geometry or the condition of the shotcrete cover. Accordingly, subsurface mineralogical conditions constitute the controlling variables (Siddique, 2024; K. Zhang, 2020; Z. Zhang et al., 2024).

Integrated interpretation of the weathering–instability continuum

Based on the three interrelated datasets (Table 4), the following was observed: First, the foliated metamorphic rock at the site was exposed to intense tropical weathering. Second, alteration proceeded preferentially along the foliation planes, grain boundaries, and microfractures. Third, primary silicate phases were progressively overprinted by chlorite, sericite, and muscovite, especially in ST-02. Fourth, this reorganization reduces cohesion and intensifies anisotropy by replacing interlocking crystalline

contacts with phyllosilicate-rich planes (Geng et al., 2023; Guo et al., 2024; Kang et al., 2025). Fifth, resistivity measurements identified a low-conductivity zone at 10–60 m depth, consistent with a weathered and fluid-influenced weak domain. Finally, although shotcrete stabilized the surface expression of the slope, it did not arrest the deeper mineralogical degradation. Therefore, the failure mechanism is internally driven, fabric-controlled, and depth-dependent. It is not simply a response to unfavorable geometry or external forcing but a consequence of progressive mineralogical transformation within the rock mass.

Table 4. Comparison of mechanical implications between samples ST-01 and ST-02

Sample	Petrographic character	XRD signature	Mechanical implication
ST-01	Wollastonite–actinolite fabric with chlorite and sericite along foliation and fractures	Albite 19.74%, chlorite 14.24%, quartz 3.16%, magnetite 3.16%, unidentified ~20.56%	Transitional alteration; cohesion reduced along planes of weakness, but interlocking still partly preserved
ST-02	Denser foliation with muscovite–chlorite alignment and stronger sericite overprint	Albite 11.61%, quartz 5.87%, muscovite 3.52%, chlorite 2.68%, magnetite 1.46%, unidentified ~20.28%	More advanced reorganization; stronger anisotropy and lower internal shear resistance

This synthesis shows in Table 4, indicates that slope failure is best understood as the outcome of a coupled process: mineralogical transformation at the grain scale, anisotropic weakening at the fabric scale, and conductive subsurface alteration at the slope scale. The data do not support a model in which the surface shotcrete alone determines stability. Instead, they indicate that critical degradation occurs beneath the reinforced layer, where weathering has already reorganized the rock mass into a weaker and more directionally sensitive state. This is why the exposed slope may appear stabilized while the supporting substrate continues to deteriorate (Garcia et al., 2017; Lasantha & Athapaththu, 2024).

Implications for engineering interpretation

For slope assessment in tropical metamorphic terrains, the Jayapura case indicates that surface inspection is insufficient. A reinforced slope should not be treated as mechanically secure simply because the shotcrete face remains visually intact. Where foliation-controlled alteration is present, the internal condition of the rock mass can differ substantially from that of the exposed surface. In practical terms, mineralogical indicators such as chlorite enrichment, muscovite alignment, sericite coatings, and unresolved low-crystallinity fractions above 20% should be treated as warning signals. Likewise, low resistivity intervals in the 10–20 Ωm range should prompt closer investigation because they may correspond to altered, fracture-rich, or clay-influenced zones that no longer provide reliable load-bearing continuity. Therefore, integrating petrography, XRD, and resistivity offers a more defensible framework for identifying hidden weak zones before failure develops (Birhanu et al., 2024; Rösche et al., 2022; K. Zhang, 2020).

The broader implication is that the rock mass quality in such slopes should be treated as time dependent rather than fixed. Weathering changes the mineral assemblage, fabric, and electrical response of the subsurface (Liang et al., 2023; Mansard et al., 2018; Yang et al., 2026). Once this transformation begins, reinforcement strategies that focus only on the surface are likely to underperform. The Jayapura Ring Road failure demonstrates that a slope can remain externally protected while the internal mechanical continuity declines. For engineering practice, this means that design and remediation should account for deeper alteration horizons, not merely visible detachment or surface cracking. In foliated metamorphic settings, the decisive instability often begins below the interface where the shotcrete ends and the weathered rock continues.

CONCLUSION

The combined petrographic, XRD, and resistivity evidence indicates that slope instability along the Jayapura City Ring Road is controlled by subsurface mineralogical transformation rather than surface deterioration, with a clear transition from a wollastonite–actinolite-supported framework in ST-01 (albite 19.74%, chlorite 14.24%) to a phyllosilicate-dominated fabric in ST-02 characterized by muscovite sericite enrichment and reduced albite (11.61%), accompanied by a persistent unresolved fraction exceeding 20% that likely represents poorly crystalline alteration products. This transformation

concentrates along the foliation and fracture networks, producing anisotropic mechanical behavior and a measurable reduction in cohesion, while resistivity values of 10–20 Ωm at depths of 10–60 m delineate a conductive and structurally weakened zone beneath the shotcrete layer. These findings contribute to the literature by demonstrating that mineralogical reorganization, rather than bulk mineral loss alone, governs the shift from intergranular load transfer to plane-controlled deformation in weathered metamorphic slopes and by linking unresolved XRD fractions with subsurface geophysical anomalies as indicators of hidden mechanical degradation. From a practical standpoint, the results suggest that slope assessment protocols relying on surface conditions or geometric stability are insufficient in foliated terrains; instead, integrated mineralogical–geophysical diagnostics should be incorporated into design standards and monitoring strategies to identify weak zones below the reinforcement depth, where failure initiation is more likely to occur.

ACKNOWLEDGMENTS

The authors gratefully acknowledge the financial support provided by the PNPB Grant, Faculty of Engineering, Cenderawasih University, for the Fiscal Year 2025, which made this research possible.

AUTHOR CONTRIBUTIONS

E.K. and E.H.: Supervision, Conceptualization, Methodology, Validation; R.I. and N.A.A.: Software, Investigation, Translation; D.P. and M.N.J.: Formal Analysis, Resources, Data Curation; J.J.: Writing – Original Draft Preparation, Writing – Review & Editing

CONFLICTS OF INTEREST

The authors declare no conflict of interest.

REFERENCES

Adjo, F. B., Bolarinwa, T. A., Adissin Glodji, L., Nude, P. M., Anagonou, B., & Olajide-Kayode, J. O. (2021). Petrographic, geochemical and structural characteristics of gold-bearing metasedimentary rocks from the Atacora structural unit, Northwestern Bénin Republic. *Arabian Journal of Geosciences*, *14*(8), 734. https://doi.org/10.1007/s12517-021-07014-5

Arango-Escobar, J. E., Toro-Toro, L. M., Moreno-Sánchez, M., & Ruíz-Jiménez, E. C. (2021). Petrography and tectonic evolution of schists of the Arquía Complex, west of Manizales in the La Manuela sector, roads Palestina and Chinchiná, Colombia. *Boletin de Geologia*, *43*(3), 63–86. https://doi.org/10.18273/revbol.v43n3-2021003

Astakhova, N. V., Ivanov, V. V., & Aksentov, K. I. (2021). Petrogeochemistry and Ore Mineralization of Sericite–Quartz Schists of the Southern Slope of the Kashevarov Bank (Sea of Okhotsk). *Oceanology*, *61*(5), 701–713. https://doi.org/10.1134/S0001437021050027

Aydan, Ö., KIyota, R., Iwata, N., & Malistani, N. (2023). Tilting and Stick–Slip Tests for Evaluating Static and Dynamic Frictional Properties of Rock Discontinuities. *Rock Mechanics and Rock Engineering*, *56*(12), 8607–8622. https://doi.org/10.1007/s00603-023-03503-z

Baldermann, A., Dietzel, M., & Reinprecht, V. (2021). Chemical weathering and progressing alteration as possible controlling factors for creeping landslides. *Science of the Total Environment*, *778*. https://doi.org/10.1016/j.scitotenv.2021.146300

Barajas-Olalde, C., Adams, D. C., Curcio, A., Davydycheva, S., Klapperich, R. J., Martinez, Y., Paembonan, A. Y., Peck, W. D., Strack, K., & Soupios, P. (2023). Application of Electromagnetic Methods for Reservoir Monitoring with Emphasis on Carbon Capture, Utilization, and Storage. *Minerals*, *13*(10), 1308. https://doi.org/10.3390/min13101308

Birhanu, B., Chemeda, Y. C., Garo, T., & Karuppannan, S. (2024). Evaluation of watertightness and slope stability analysis of Upper Guder dam, West Showa, Central Ethiopia. *Quaternary Science Advances*, *15*, 100230. https://doi.org/10.1016/j.qsa.2024.100230

Bonnet, M., Robin, V., Parrotin, F., Grozeva, N., Seigneur, N., Batbaatar, M.-E., & Descostes, M. (2024). Influence of clay minerals on pH and major cation concentrations in acid-leached sands: Column

experiments and reactive-transport modeling. *Journal of Contaminant Hydrology*, *264*, 104363. https://doi.org/10.1016/j.jconhyd.2024.104363

Castillo-Reyes, O., Jiménez-Andrade, J. L., Dehiya, R., & Iturrarán-Viveros, U. (2025). Inverse geo-electromagnetic modeling: A systematic review and bibliometric assessment. *Frontiers in Earth Science*, *13*, 1645896. https://doi.org/10.3389/feart.2025.1645896

Chen, W., Wan, W., Zhao, Y., Xie, S., Jiao, B., Dong, Z., Wang, X., & Lian, S. (2020). Aging features and strength model of diorite's damage considering acidization. *Frontiers in Physics*, *8*, 553643. https://doi.org/10.3389/fphy.2020.553643

Cui, Y., Zhang, H., Liu, T., Yang, Z., Zhang, Y., & Ling, X. (2025). Mechanical Performance Degradation and Microstructural Evolution of Grout-Reinforced Fractured Diorite Under High Temperature and Acidic Corrosion Coupling. *Buildings*, *15*(19), 3547. https://doi.org/10.3390/buildings15193547

De Oliveira Frascá, M. H. B. (2018). Petrographic Analysis. In P. T. Bobrowsky & B. Marker (Eds.), *Encyclopedia of Engineering Geology* (pp. 705–713). Springer International Publishing. https://doi.org/10.1007/978-3-319-73568-9_218

Döbelin, N. (2020). Validation of XRD phase quantification using semi-synthetic data. *Powder Diffraction*, *35*(4), 262–275. https://doi.org/10.1017/S0885715620000573

Erharter, G. H. (2024). Rock Mass Structure Characterization Considering Finite and Folded Discontinuities: A Parametric Study. *Rock Mechanics and Rock Engineering*, *57*(7), 5229–5249. https://doi.org/10.1007/s00603-024-03787-9

Garcia, C., Castellanos, O., & Figueroa, L. C. M. (2017). Petrology, geochemistry and geochronology of the arquía complex́s metabasites at the Pijao-Génova sector, Central Cordillera, Colombian Andes. *Boletín de Geología*, *39*(1), 105–126. https://doi.org/10.18273/revbol.v39n1-2017005

Geng, W., Wang, J., Zhang, X., Huang, G., Li, L., & Guo, S. (2023). Experimental study of pore structure and rock mechanical properties of tight sandstone after acid treatment. *Acta Geotechnica*, *18*(12), 6559–6571. https://doi.org/10.1007/s11440-023-02094-x

Gofar, N., Haryanto, Y., & Purnama Sari Dewi, A. (2025). Identification of rainfall scenario triggering slope failures in Pagar Alam and its surrounding area. *Media Komunikasi Teknik Sipil*, *30*(2), 256–264. https://doi.org/10.14710/mkts.v30i2.62372

Grayver, A. (2024). Unravelling the Electrical Conductivity of Earth and Planets. *Surveys in Geophysics*, *45*(1), 187–238. https://doi.org/10.1007/s10712-023-09813-9

Guo, S., Zhang, X., Wang, J., Wang, S., Liu, K., & Wang, J. (2024). Deeply buried clastic rock diagenesis evolution mechanism of Dongdaohaizi sag in the center of Junggar fault basin, Northwest China. *Open Geosciences*, *16*(1), 20220711. https://doi.org/10.1515/geo-2022-0711

Habimana, E., & Sauvé, S. (2025). A review of properties, occurrence, fate, and transportation mechanisms of contaminants of emerging concern in sewage sludge, biosolids, and soils: Recent advances and future trends. *Frontiers in Environmental Chemistry*, *6*, 1547596. https://doi.org/10.3389/fenvc.2025.1547596

Kang, Z., Liangwei, L., Kun, L., Shaojie, Z., & Zhizhong, J. (2025). Study on the effect of acid fracturing fluid on pore structure of middle to high rank coal. *Scientific Reports*, *15*(1), 2097. https://doi.org/10.1038/s41598-024-85007-6

Kiselnikov, Y. V., Perova, E. N., Proskurnin, V. F., & Shneider, A. G. (2026). Conditions of Metamorphism of The Host Rocks in The Borzova River Gold Ore Cluster (Northeastern Taimyr). *Russian Geology and Geophysics*, *67*(3), 376–392. https://doi.org/10.2113/RGG20254868

Lasantha, H. S., & Athapaththu, A. M. R. G. (2024). Multidisciplinary Slope Stability Assessment in Weathered Metamorphic Rocks: A Case Study of the Highland Complex, Sri Lanka. *Geotechnical and Geological Engineering*, *42*(7), 6027–6050. https://doi.org/10.1007/s10706-024-02868-4

Liang, F., Hinderer, M., & Hornung, J. (2023). Quantification of physical and chemical paleoweathering at the microscale: A new concept. *International Journal of Earth Sciences*, *112*(3), 1063–1090. https://doi.org/10.1007/s00531-022-02281-3

Liu, B., Yang, H., Haque, E., & Wang, G. (2021). Effect of Joint Orientation on the Breakage Behavior of Jointed Rock Mass Loaded by Disc Cutters. *Rock Mechanics and Rock Engineering*, *54*(4), 2087–2108. https://doi.org/10.1007/s00603-021-02379-1

Liu, J., Guan, Y., Shao, Z., & Wang, H. (2022). Mechanical effect of clay under the acid-base action: A case study on montmorillonite and illite. *Frontiers in Earth Science*, *10*, 991776. https://doi.org/10.3389/feart.2022.991776

Mader, T., Schreter, M., & Hofstetter, G. (2022). On the Influence of Direction-Dependent Behavior of Rock Mass in Simulations of Deep Tunneling Using a Novel Gradient-Enhanced Transversely Isotropic Damage–Plasticity Model. *Applied Sciences*, *12*(17), 8532. https://doi.org/10.3390/app12178532

Mansard, N., Raimbourg, H., Augier, R., Précigout, J., & Le Breton, N. (2018). Large-scale strain localization induced by phase nucleation in mid-crustal granitoids of the south Armorican massif. *Tectonophysics*, *745*, 46–65. https://doi.org/10.1016/j.tecto.2018.07.022

Maruyama, S., Suzuki, K., & Liou, J. G. (1983). Greenschist-Amphibolite Transition Equilibria at Low Pressures. *Journal of Petrology*, *24*(4), 583–604. https://doi.org/10.1093/petrology/24.4.583

McAleer, R. J., Bish, D. L., Kunk, M. J., Sicard, K. R., Valley, P. M., Walsh, G. J., Wathen, B. A., & Wintsch, R. P. (2017). Reaction softening by dissolution–precipitation creep in a retrograde greenschist facies ductile shear zone, New Hampshire, USA. *Journal of Metamorphic Geology*, *35*(1), 95–119. https://doi.org/10.1111/jmg.12222

Mitchell, A., & Sass, O. (2024). Rock weathering: The effects of varying rock moisture on controlled weathering cycles in low porosity limestone. *Geomorphology*, *457*, 109149. https://doi.org/10.1016/j.geomorph.2024.109149

Mu, J., Zhao, S., Brzozowski, M., Li, H., Wu, C., & Li, W. (2023). Geology, geochemistry and genesis of the world-class Shizhushan wollastonite deposit, Mengshan area, South China. *Ore Geology Reviews*, *158*, 105469. https://doi.org/10.1016/j.oregeorev.2023.105469

Nzeukou, A. N., Tsozué, D., Bomeni, I. Y., Mache, J. R., Kwopnang, M. R., & Fagel, N. (2024). Clay mineralogy in mylonite weathering products from Njimom (west Cameroon): Origin and terracotta suitability. *Discover Geoscience*, *2*(1), 69. https://doi.org/10.1007/s44288-024-00078-2

Park, J. Y., Jo, Y., Koo, H. J., Um, I. K., & Lee, K. (2026). Machine-learning-based semi-quantitative analysis model of clay minerals in Onsan–Busan coastal sediments, South Korea. *Geosciences Journal*. https://doi.org/10.1007/s12303-026-00091-2

Phyu, H. T., Hendrayana, H., Indrawan, I. G. B., & Kamai, T. (2021). Simulation of Kalirejo Road Side Slope based on Altered Andesite Characters, Kulon Progo Regency, Indonesia. *Journal of Applied Geology*, *5*(2), 101. https://doi.org/10.22146/jag.56916

Price, C. (2016). ELF Electromagnetic Waves from Lightning: The Schumann Resonances. *Atmosphere*, *7*(9), 116. https://doi.org/10.3390/atmos7090116

Regmi, A. D., Yoshida, K., Dhital, M. R., & Devkota, K. (2013). Effect of rock weathering, clay mineralogy, and geological structures in the formation of large landslide, a case study from Dumre Besei landslide, Lesser Himalaya Nepal. *Landslides*, *10*(1), 1–13. https://doi.org/10.1007/s10346-011-0311-7

Rösche, C., Waeselmann, N., Petrova, N., Malcherek, T., Schlüter, J., & Mihailova, B. (2022). Oxidation processes and thermal stability of actinolite. *Physics and Chemistry of Minerals*, *49*(12), 47. https://doi.org/10.1007/s00269-022-01223-4

Siddique, T. (2024). Rock mass classification in slope engineering with special emphasis on Slope mass rating: Current status and future projections. *Geological Journal*, *59*(9), 2472–2486. https://doi.org/10.1002/gj.4933

Sirbu-Radasanu, D. S., Huzum, R., Dumitraş, D.-G., & Stan, C. O. (2022). Mineralogical and Geochemical Implications of Weathering Processes Responsible for Soil Generation in Mănăila Alpine Area (Tulgheş 3 Unit—Eastern Carpathians). *Minerals*, *12*(9), 1161. https://doi.org/10.3390/min12091161

Starr, P. G., & Pattison, D. R. M. (2019). Metamorphic devolatilization of basalts across the greenschist-amphibolite facies transition zone: Insights from isograd mapping, petrography and thermodynamic modelling. *Lithos*, *342–343*, 295–314. Scopus. https://doi.org/10.1016/j.lithos.2019.05.020

Sun, Q., Lyu, C., & Zhang, W. (2020). The relationship between thermal conductivity and electrical resistivity of silty clay soil in the temperature range − 20 C to 10 C. *Heat and Mass Transfer*, *56*(6), 2007–2013. https://doi.org/10.1007/s00231-020-02813-0

Taivalkoski, A., Ranta, J.-P., Sarala, P., Moilanen, M., Nikkola, P., & Soukka, T. (2024). Pyrite-goethite alteration in supergene oxidation processes in till: Elemental distribution and evaluation of goethite usability as a fingerprinting tool for vectoring mineral deposits. *Minerals*, *14*(7), 668. https://doi.org/10.3390/min14070668

Tang, J., Taro, U., Huang, D., Xie, J., & Tao, S. (2020). Physical Model Experiments on Water Infiltration and Failure Modes in Multi-Layered Slopes under Heavy Rainfall. *Applied Sciences*, *10*(10), 3458. https://doi.org/10.3390/app10103458

Tao, G., Liu, R., Zhang, P., Wang, Y., Zuo, L., & Zhang, X. (2024). Carbonate nanoparticles formed by water–rock reactions in groundwater: Implication of carbonate rock weathering in carbonate aquifers. *Minerals*, *14*(10), 980. https://doi.org/10.3390/min14100980

Uzarowicz, Ł., Šegvić, B., Michalik, M., & Bylina, P. (2012). The effect of hydrochemical conditions and pH of the environment on phyllosilicate transformations in the weathering zone of pyrite-bearing schists in Wieśiszowice (SW Poland). *Clay Minerals*, *47*(4), 401–417. https://doi.org/10.1180/claymin.2012.047.4.01

Wang, H., Liu, F., Ji, L., Tian, Z., Xu, W., & Liu, L. (2019). Petrology, geochemistry and metamorphic evolution of Lancang Group in the Changning-Menglian complex belt and its implications on the tectonic evolution of the Paleo-Tethys. *Yanshi Xuebao/Acta Petrologica Sinica*, *35*(6), 1773–1799. https://doi.org/10.18654/1000-0569/2019.06.09

Wang, J., Chen, J., Shi, Y., Cheng, N., Tang, G., Peng, C., Tang, J., & Li, J. (2025). Petrogenesis and tectonic implications of blueschist-facies garnet-mica schist in the Dabie orogenic belt, central China. *Journal of Asian Earth Sciences*, *280*. Scopus. https://doi.org/10.1016/j.jseaes.2024.106482

Wang, Y., Liu, X., & Li, Q. (2022). Pyrite oxidation under a carbonate buffer and its environmental implications: A case study from the Shangmanggang gold deposit, SW China. *Geochemistry: Exploration, Environment, Analysis*, *22*(4). https://doi.org/10.1144/geochem2022-021

Waqas, U., Qureshi, M. U., Saqib, S., Rashid, H. M. A., & Rasool, A. M. (2024). Evaluation of Strength Anisotropy in Foliated Metamorphic Rocks: A Review Focused on Microscopic Mechanisms. *Geosciences*, *14*(10), 253. https://doi.org/10.3390/geosciences14100253

Xiao, J., Song, Y., & Li, Y. (2023). Comparison of Quantitative X-ray Diffraction Mineral Analysis Methods. *Minerals*, *13*(4), 566. https://doi.org/10.3390/min13040566

Yamasaki, S., & Chigira, M. (2007). *Water-rock interactions during the weathering of pelitic schist—Its role in the development of landslides*. *2*, 1435–1438. Scopus. https://doi.org/10.1201/noe0415451369.ch302

Yan, S., Wang, Q., Wang, H., Qiu, S., Zeng, Z., & Fang, Y. (2020). Strength control factors of chlorite schist under schistose structure. *International Journal of Design and Nature and Ecodynamics*, *15*(5), 631–637. https://doi.org/10.18280/ijdne.150503

Yang, J., Xu, G., Zhou, Y., Shu, Y., Chen, Z., Zhang, C., & Zhang, J. (2026). Laboratory experimental and three-dimensional numerical study of anisotropic behavior of schist under triaxial compression experiment conditions. *Computers and Geotechnics*, *195*. Scopus. https://doi.org/10.1016/j.compgeo.2026.108054

Yin, X., Huang, Y., Zhang, A., & Lei, Y. (2023). Effect of Fabric Factors on the Mechanical Behavior of Foliated Rocks: A Particle Flow Approach. *Geotechnical and Geological Engineering*, *41*(2), 1031–1047. https://doi.org/10.1007/s10706-022-02321-4

You, Z., Yang, W., Tian, H., Zhou, Y., Zhao, L., Yao, C., Yan, Q., & Deng, L. (2026). Strength evolution and failure behavior in schistose basalt under varying stress and schistosity plane dip angle. *Transportation Geotechnics*, *56*. https://doi.org/10.1016/j.trgeo.2025.101804

Zalooli, A., Khamehchiyan, M., Nikudel, M. R., Fort, R., Ghasemi, S., & Freire-Lista, D. M. (2024). The Influence of Petrographic Properties on Mechanical Characteristics and the Durability of the Greenschist Subjected to Simulated Weathering Tests. *Rock Mechanics and Rock Engineering*, *57*(5), 3393–3408. https://doi.org/10.1007/s00603-023-03735-z

Zhang, H., Liu, T., Wang, W., Cui, Y., & Zhang, D. (2025). Experimental Study on Multiscale Damage Mechanism of Diorite Under the Effects of High Temperature and Acidic Environment. *Rock Mechanics and Rock Engineering*. https://doi.org/10.1007/s00603-025-05058-7

Zhang, K. (2020). Three-Dimensional Effect and Strength Reduction Method. In K. Zhang, *Failure Mechanism and Stability Analysis of Rock Slope* (pp. 159–183). Springer Singapore. https://doi.org/10.1007/978-981-15-5743-9_8

Zhang, X.-Z., Dong, Y.-S., Wang, Q., Dan, W., Zhang, C., Xu, W., & Huang, M.-L. (2017). Metamorphic records for subduction erosion and subsequent underplating processes revealed by garnet-staurolite-muscovite schists in central Qiangtang, Tibet. *Geochemistry, Geophysics, Geosystems*, *18*(1), 266–279. https://doi.org/10.1002/2016GC006576

Zhang, Z., Shi, X., Qiu, X., Ouyang, J., & Wang, W. (2024). In Situ Tests Comparing the Support Effects of Thin Spray-on Liner and Shotcrete on a Roadway Subjected to Blasting. *Rock Mechanics and Rock Engineering*, *57*(3), 1669–1693. https://doi.org/10.1007/s00603-023-03654-z

Zheng, Z., Gao, S., Li, X., Huang, X., Qiu, S., & Liu, X. (2026). Shear Mechanical Behaviors and Cracking Evolution Mechanism of Foliated Rock Under Tunnel Excavation Disturbance Conditions. *Rock Mechanics and Rock Engineering*. https://doi.org/10.1007/s00603-025-05202-3

Zhou, Y., Su, S., Li, P., & Suo, W. (2020). Mechanical properties 01 chlorite phylhteand its degradation mechanism under saturated state. *Chinese Journal of Geological Hazard and Control*, *31*(1), 95–101. Scopus. https://doi.org/10.16031/j.cnki.issn.1003-8035.2020.01.15